Supporting Information

Effect of Natural Organic Matter (NOM) on the Removal Efficiency of Hg(II) by MoS_2: Dependence on the Hg/MoS_2 Ratio and NOM Properties

Mengxia Wang[a,b], Meng Zhang[b], Qi Han[b], Xun Liu[a,b], Yufei Shu[b], Beizhao Chen[b], Yuchao Chen[b], Bei Liu[b*], Zhongying Wang[b,c*]

[a] School of Environment, Harbin Institute of Technology, Harbin 150001, China
[b] School of Environmental Science and Engineering
Southern University of Science and Technology, Shenzhen 518055, China
[c] Guangdong Provincial Key Laboratory of Soil and Groundwater Pollution Control, School of Environmental Science and Engineering, Southern University of Science and Technology, Shenzhen 518055, China

[*] to whom correspondence should be addressed.
e-mail: liub@sustech.edu.cn;
e-mail: wangzy6@sustech.edu.cn;

Table Contents

Text S1. Characterizations

The hydrodynamic size and zeta potential (ζ) of the MoS_2 nanosheets were determined using a Zetasizer instrument (NanoBrook Omini, Brookhaven, U.S.A.). For the size of MoS_2 testing, about 2 mL 30 mg/L of MoS_2 aqueous solution were added to plastic cell and according to the Stokes-Einstein formula to calculate the particle size. For the zeta potential (ζ) of the MoS_2 nanosheets testing, the palladium electrode was inserted into a quartz cell with 2 mL 30 mg/L of MoS_2 diluted with ultrapure water, based on the Smoluchowski formula to obtain the zeta potential value of MoS_2.

The morphologies of the MoS_2 nanosheets were characterized using transmission electron microscopy (TEM, Talos F200X, FEI, U.S.A.) and atomic force microscopy (AFM, MFP-3D Stand Alone, Asylum Research, U.S.A.). The exfoliated MoS_2 nanosheets were dispersed in ethanol and ultrasonicated for 10 min. Before TEM testing, the sample was firstly dropped onto the copper grid with carbon support and dried to keep the residual particles attached to the grid. Subsequently, the sample was measured by a microscope equipped with a Schottky emitter gun operated (at 200 kV). For AFM testing, the distributed MoS_2 nanosheets in ethanol were dropped onto a silicon wafer, then measured with an AC mode through Micro Cantilevers probe tip (240AC-NA, 70 kHz 2N/m) and AFM image was obtained by MFP-3D Stand Alone.

X-ray photoelectron spectroscopy (XPS, PHI 5000 Versaprobe III spectrometer, ULVAC-PHI, Japan) and Raman spectrometer (HORIBA LabRAM HR Evolution, Japan) were used to analyze the phase and chemical composition of the MoS_2 nanosheets. The samples were collected by filtration, and then dried in a vacuum freeze-

tryer. For XPS testing, the samples were firstly deposited on conductive adhesive, then using high-resolution scans with a PHI 5000 VersaProbe III equipped with a monochromatic Al anode (Al Kα = 1486.7 eV) as an X-ray source to measured. For Raman testing, the samples were firstly deposited on glass slides, the spectra recorded by s LabRAM HR Evolution micro confocal Raman spectrometer with a 532 nm excitation laser. To real the complexation of Hg and NOM, solution-phase attenuated total reflectance Fourier Transform Infrared (ATR-FTIR) (Bruker Vertex 70v, Germany) spectroscopy measurements were conducted before and after Hg complexation with NOM through a diamond sample stage.

Text S2. Mercury uptake isotherms with different NOM concentration

Batch uptake isotherm tests were performed in the same Teflon vials, maintaining a fixed MoS_2 concentration of 4 mg/L, while varying initial Hg concentration from 0 to 45 mg/L and the NOM concentration at 0, 3, and 20 mg/L. After 24 hours of equilibration, the samples were filtered through 0.22 μm PTFE filters, and the filtrates were analyzed with a direct mercury analyzer (DMA-80, Milestone, Italy). The isotherm data was fitted with the classical Langmuir model (**Eq. (1)**):

$$q_e = \frac{q_m K_L C_e}{1 + K_L C_e} \tag{1}$$

where q_e (mg/g) and C_e (mg/L) are the equilibrium Hg uptake capacity and the equilibrium Hg concentration, q_m (mg/g) is the maximum removal capacity, K_L (L/mg) is the Langmuir affinity constant.

Text S3. Separate Hg-NOM with the Amico Ultra-15 centrifugal filters

In order to quantify the Hg complexation by different fraction of NOM, an ultrafiltration membrane was used to separate Hg-NOM and free Hg. Firstly, a series of Amico Ultra-15 centrifugal filters with decreasing molecular weight cut-offs (MWCO) of 100 KDa, 30 KDa, 10 KDa, and 3 KDa were used to separate pristine NOM for obtained NOM MW fractionation (i.e., > 100 KDa, 30–100 KDa, 10–30 KDa, 3–10 KDa, <3 KDa). Subsequently, NOM with different molecular weights (> 100 KDa, 30–100 KDa, 10–30 KDa, 3–10 KDa) is mixed with Hg (10 mg/L of TOC, 0.5 mg/L of Hg), and then subjected to centrifugation in their respect MWCO membrane. The concentration of Hg in filtrate was determined by a direct mercury analyzer. In the control experiment, Hg solution without NOM was filtered by ultrafiltration membranes in the same condition.

Table S1. Pseudo-first-order and pseudo-second-order models for simulating Hg removal kinetics and the corresponding parameters.

NOM concentration (mg/L)	Kinetic models	Parameters		R^2
0	Pseudo-first-order	K_1 (h^{-1}) 0.37	q_e (mg/g) 3053.4	0.987
	Pseudo-second-order	K_2 (g/(mg•h)) 0.002	q_e (mg/g) 5000	0.999
20	Pseudo-first-order	K_1 (h^{-1}) 0.7	q_e (mg/g) 1032.6	0.89
	Pseudo-second-order	K_2 (g/(mg•h)) 0.0005	q_e (mg/g) 2000	0.996

Table S2. Regression parameters of sorption isotherm data of Hg onto MoS_2 nanosheets by Langmuir models in the presence of NOM.

NOM concentration (mg/L)	Parameters		R^2
0	q_m (mg/g) 5376.20	K_L (L/mg) 1.93	0.98
3	q_m (mg/g) 1963.40	K_L (L/mg) 20.93	0.87
20	q_m (mg/g) 1536.40	K_L (L/mg) 2.94	0.97

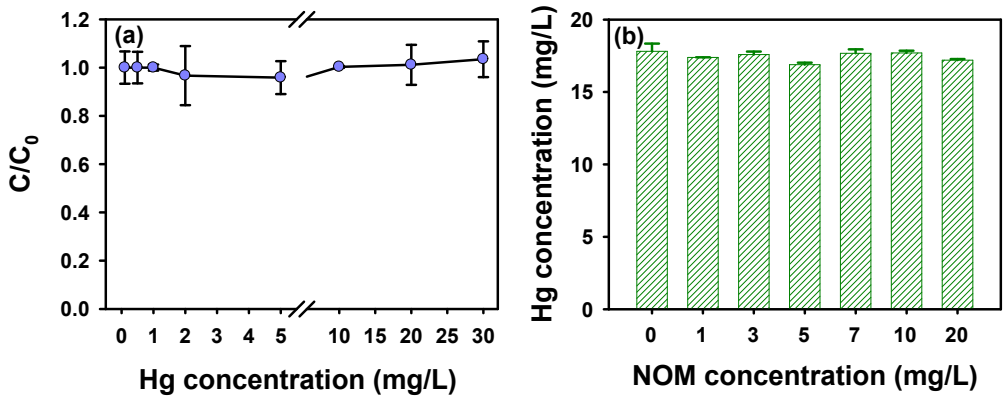

Fig. S1. The concentration of Hg in the filtrate after filtration through 0.22 μm PTFE filter: (a) at different initial Hg concentration in the absence of NOM; and (b) at different NOM addition, with the constant Hg concentration at ~18 mg/L.

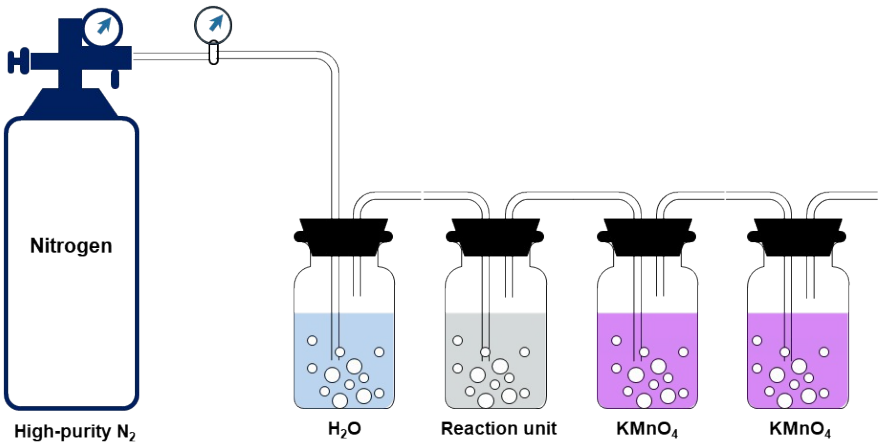

Fig. S2. The experimental set-up for Hg^0 collection. The reaction unit contained MoS_2 and Hg(II); $KMnO_4$ solution was prepared with 0.024% (w/v) $KMnO_4$ in 4% (v/v) H_2SO_4.

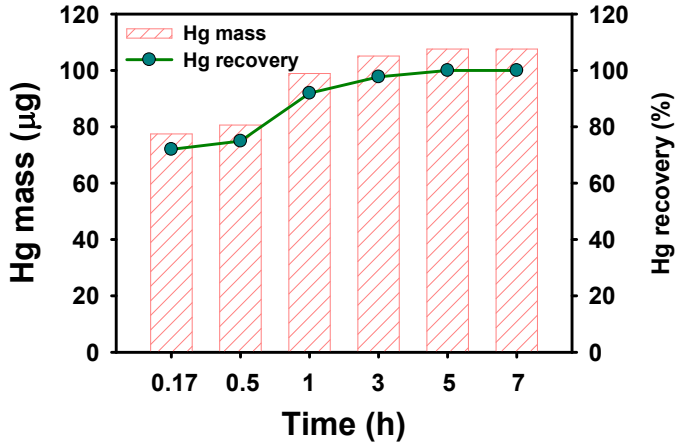

Fig. S3. The reduction of Hg(II) by $SnCl_2$ to verify the recovery efficiency of Hg in the experimental device.

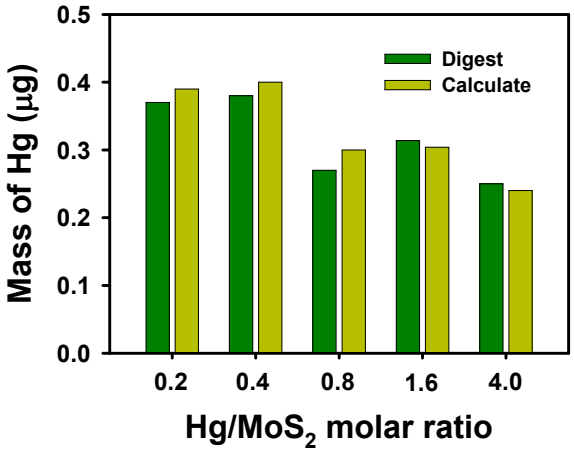

Fig. S4. Comparison of Hg in solids determined quantitatively by two methods.

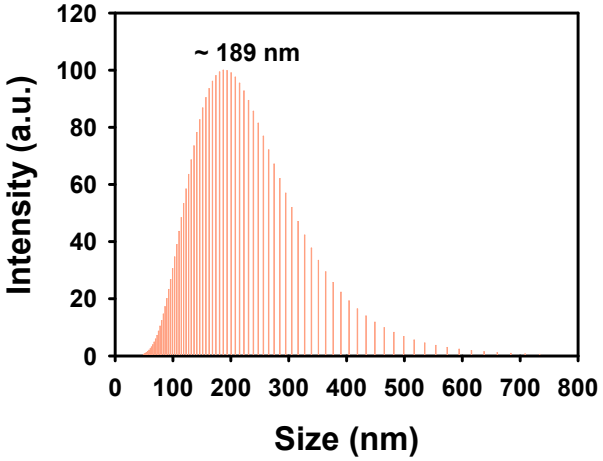

Fig. S5. The particle size distribution of the MoS_2 nanosheets.

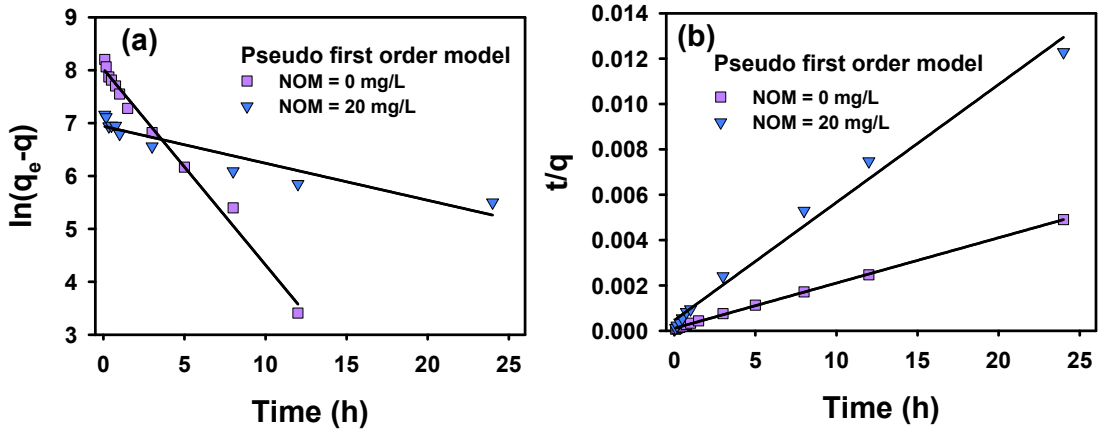

Fig. S6. Fitting results of Hg removal kinetics by Pseudo-first-order (a) and pseudo-second-order (b).

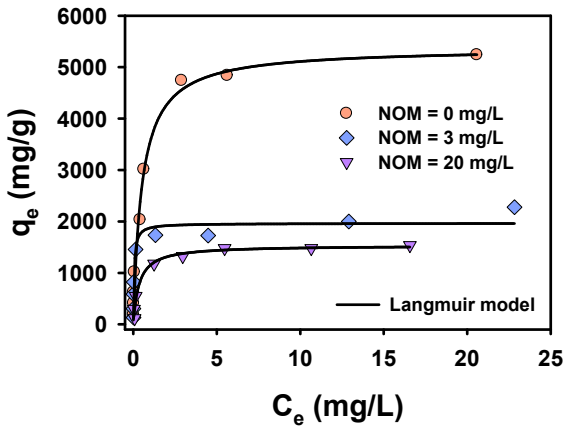

Fig. S7. Isotherm of Hg uptake by MoS_2 fitted with Langmuir model at different NOM concentration, initial Hg concentration was 0–45 mg/L, MoS_2 concentration was 4 mg/L.

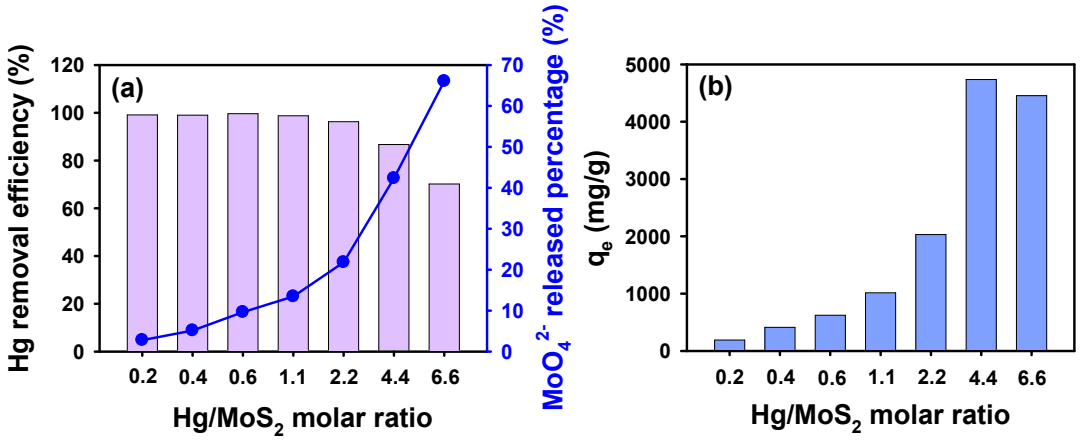

Fig. S8. (a) The removal efficiency of Hg by MoS_2 and the release of MoO_4^{2-} at various Hg/MoS_2 molar ratios. (b) The removal capacity of Hg by MoS_2 at various Hg/MoS_2 molar ratios.

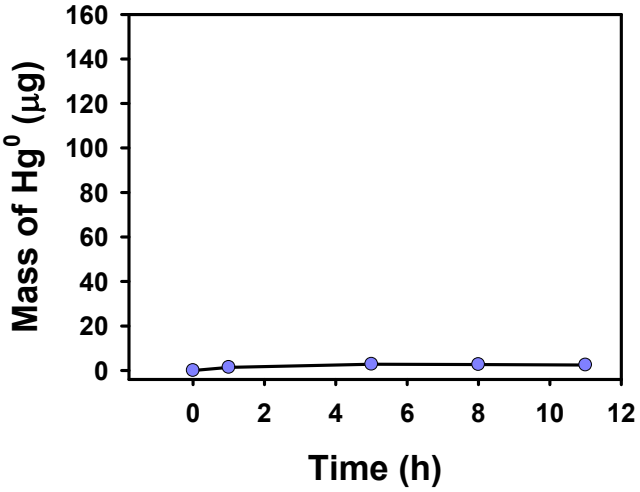

Fig. S9. The control test of Hg(II) reduced by N_2.

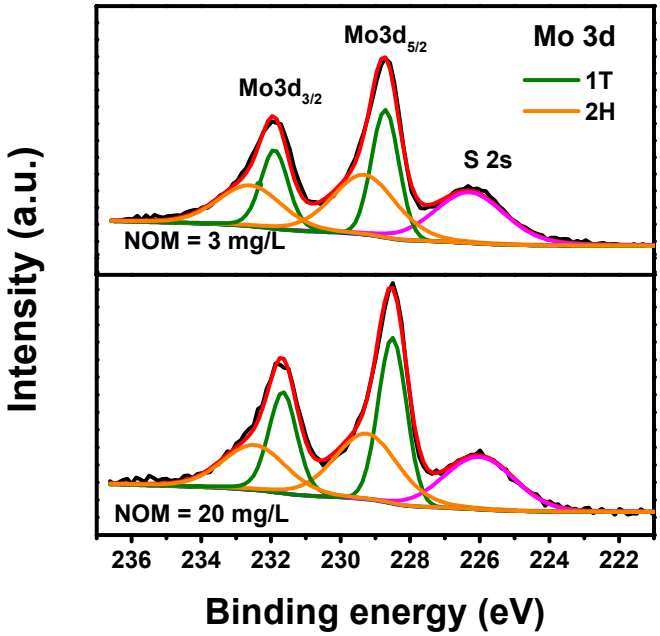

Fig. S10. Mo 3d XPS spectra of Hg-laden MoS_2 in the presence of NOM, at a Hg/MoS_2 molar ratio of 4.0.

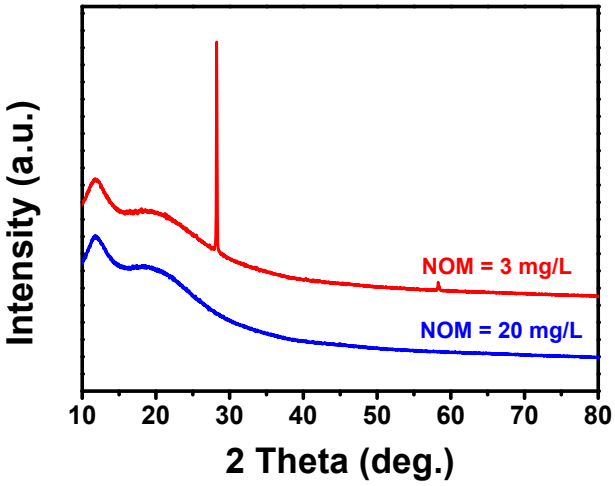

Fig. S11. XRD spectra of Hg-laden MoS_2 in the presence of NOM, at a Hg/MoS_2 molar ratio of 4.0.

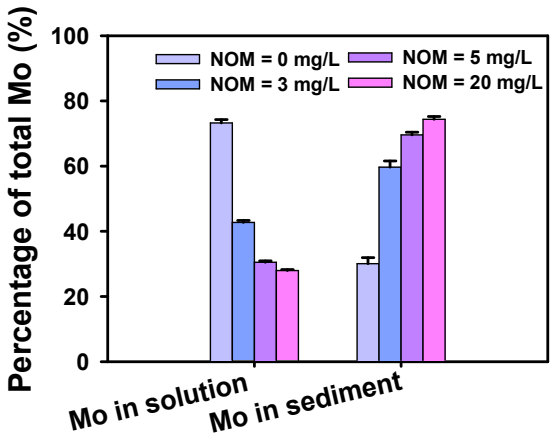

Fig. S12. The release of MoO_4^{2-} after Hg removal by MoS_2 at the Hg/MoS_2 ratio of 4.0.

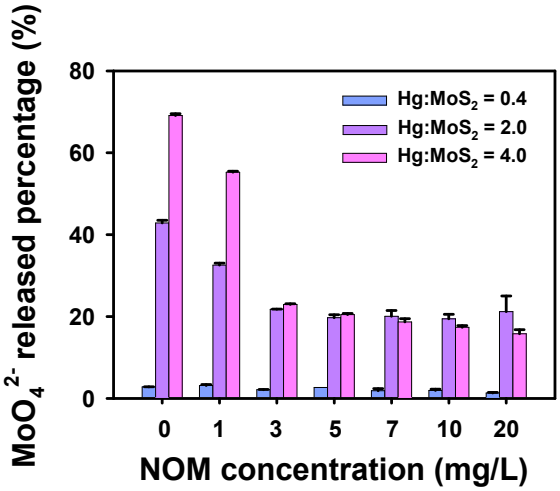

Fig. S13. The release of MoO_4^{2-} after Hg removal by MoS_2 at various Hg/MoS_2 molar ratios.

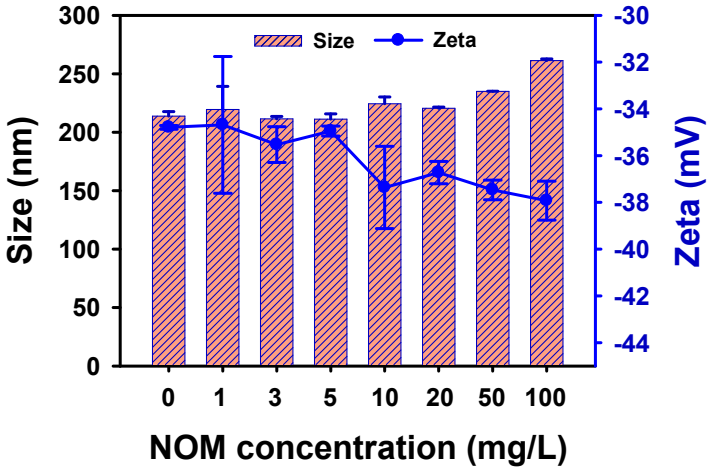

Fig. S14. Effect of NOM on the size and zeta potential of MoS_2.

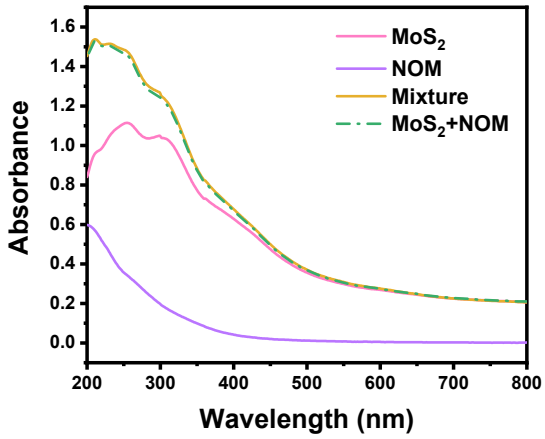

Fig. S15. Ultraviolet-vis spectra of MoS_2, NOM, and their mixture (solid lines). The dash line represents sum of the NOM and MoS_2 absorbance at each wavelength.

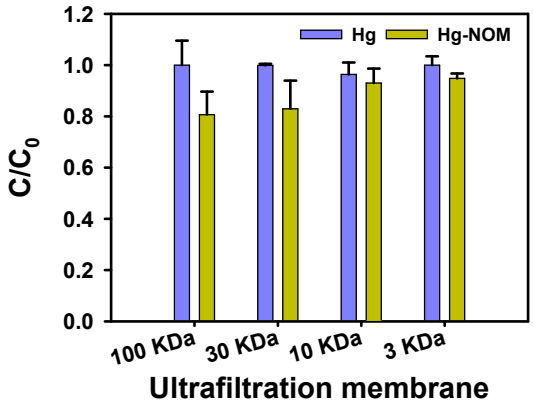

Fig. S16. The influence of different NOM fraction on Hg complexation.

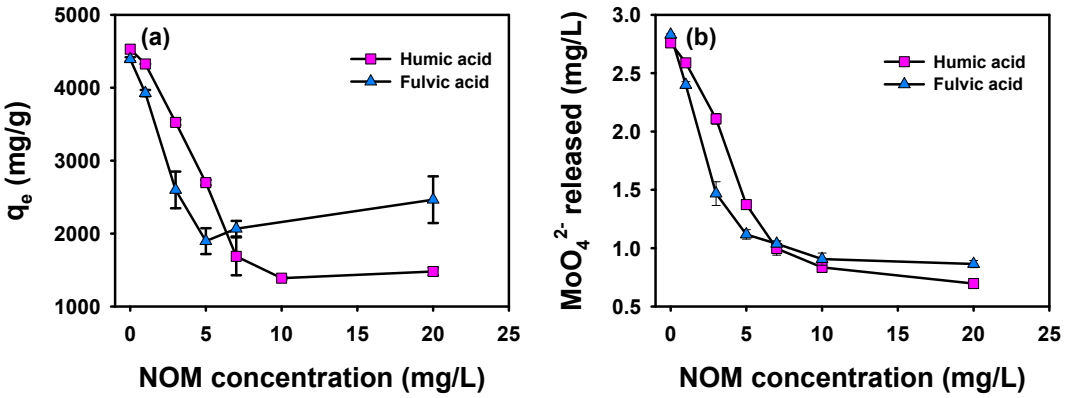

Fig. S17. Effect of HA and FA on the removal of Hg(II) by MoS_2 at a Hg/MoS_2 ratio of 4.0.